THE JOURNAL OF PHYSICAL CHEMISTRY C

pubs.acs.org/JPCC Article

Tuning Electronic and Magnetic Properties of Two-Dimensional Ferromagnetic Semiconductor CrI_3 through Adsorption of Benzene

Min Lu, Qiushi Yao, Qiongyu Li, Chuanyun Xiao, Chengxi Huang,* and Erjun Kan*

Cite This: J. Phys. Chem. C 2020, 124, 22143−22149 Read Online

ABSTRACT: Two-dimensional (2D) ferromagnetic (FM) semiconductor chromium triiodide (CrI_3) has attracted much attention because of its long-range two-dimensional (2D) FM order and tunable interlayer magnetic coupling. In the present work, the electronic and magnetic properties of CrI_3 monolayer adsorbing benzene molecules (denoted as C_6H_6@CrI_3) is systematically investigated by means of first-principles calculations, which gives a better understanding and particular opportunity of crafting desired properties of this material. It is found that the adsorption of benzene molecules can enhance the optical absorption and FM couplings of CrI_3 monolayer. The enhancement of FM coupling is independent of the adsorption concentration of benzene molecules. We hope that these findings will bring additional interest to the newly experimentally synthesized 2D FM semiconductor.

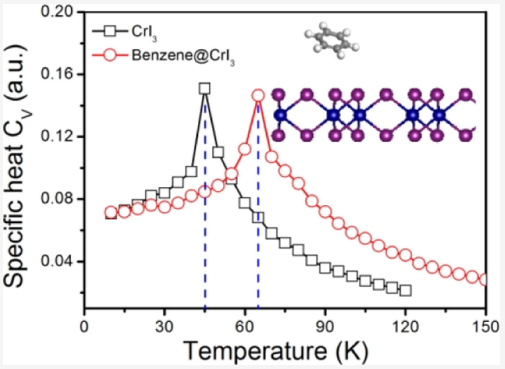

1. INTRODUCTION

Two-dimensional (2D) materials offer remarkable physical properties for potential applications in nanotechnology due to their reduced dimension and symmetry.[1,2] Ever since the discovery of graphene in 2004, a variety of 2D materials have been found to have useful electronic, optical, mechanical, and thermal properties.[3−7] 2D materials host a wealth of physical phenomena, but the realization of intrinsic 2D magnetism at finite temperature remains a challenge. It is well known that long-range magnetic order is predicted to be prohibited due to the strong fluctuations at finite temperature in a 2D system, according to the Mermin−Wagner theorem.[8] Thus, whether long-range magnetic order can exist in 2D systems remains an open question despite plenty of early first-principles predictions of 2D magnets such as chromium triiodide (CrI_3) monolayer,[9] graphitic C_4N_3,[10] ScCl,[11] Fe_2Si,[12] and Co/MoS_2[13] heterostructures. Recently, this question has been answered by the experimental discoveries of long-range ferromagnetic (FM) order in 2D intrinsic semiconductors which break the Mermin−Wagner restriction via strong magnetic anisotropy. FM ordering in few-layered $Cr_2Ge_2Te_6$ has first been successfully observed in experiments.[14] Soon after, another FM semiconductor CrI_3 down to monolayer was confirmed as the thinnest intrinsic 2D FM semiconductor material with a Curie temperature (T_c) of 45 K.[15] These findings open the door for the application of 2D magnetic materials at a nanoscale.

A number of recent studies in this field are focusing on tailoring the electronic and magnetic properties of the discovered 2D FM semiconductors.[16−20] Typically, whether a semiconductor has large magnetic moment or not significantly influences its practical application.[21] Besides, the electronic property of a semiconductor has a direct influence on the light absorption and light emission.[22−24] In general, the low T_c of pristine CrI_3 monolayer has been considered as a major obstacle for its numerous advanced applications in spin electric devices and optoelectronics.[9,25] Consequently, it is necessary to explore effective ways to realize broader developments and applications. In the past decade, it has been demonstrated that molecular doping is an effective and flexible method toward modulating the properties of 2D materials such as graphene, BN monolayer/nanoribbons, MoS_2 monolayers, silicone, and monolayer As, Sb, Bi.[26−33] On the basis of these investigations, molecular doping is expected to tune the electronic and magnetic properties of CrI_3.

In the present work, by means of first-principles calculations, we propose that the adsorption of benzene molecules on CrI_3 monolayer will dramatically influence its electronic and magnetic properties. We first studied the adsorption configurations, which shows that the adsorbed benzene molecule prefers to locate at the I-top site with a bit tilt instead of parallel to the CrI_3 plane. The adsorption energy ranges from −0.35 to −0.5 eV. Then, we demonstrate that the

Received: July 3, 2020
Revised: September 4, 2020
Published: September 10, 2020

https://dx.doi.org/10.1021/acs.jpcc.0c06071
J. Phys. Chem. C 2020, 124, 22143−22149

adsorption of benzene molecules can improve the T_C from 45 to 65 K. The enhancement of FM coupling is independent of the adsorption concentration of benzene molecules. Moreover, the feasibility of C_6H_6@CrI_3 is verified by the *ab initio* molecular dynamics (AIMD) simulations. These findings will be helpful for engineering the electronic and magnetic properties of CrI_3 monolayer and open the possibility of the application in optoelectronics.

2. COMPUTATIONAL METHODS

Our first-principles calculations were carried out by performing spin-polarized density functional theory (DFT) calculations, as implemented in the Vienna *Ab initio* Simulation Package.[34] The general gradient approximation (GGA) of Perdew−Burke−Ernzerhof (PBE) pseudopotentials[35] were used to describe the electron exchange and correlation interactions within the projector augmented wave (PAW) method.[36] For all kinds of atoms, the standard PAW_PBE pseudopotential is employed, and the valence states are treated as Cr $3d^5 4s^1$, I $5s^2 5p^5$, and C $2s^2 2p^2$. Considering the strongly electronic correlation for the partially filled d subshells, we use the GGA + *U* method introduced by Dudarev et al.[37] with U_{eff} = 3 eV for Cr-d orbitals. The effect of spin−orbit coupling (SOC) was also introduced for the calculations of electronic band structures. A plane-wave basis set with an energy cutoff of 500 eV was used. The Γ-centered Monkhorst−Pack[38−40] point scheme with 8 × 8 × 1 grid meshes is used to sample the reciprocal space of the primitive cell. In order to achieve an accurate description of weak interactions, the DFT-D3 method by Grimme[41,42] is used to account for the van der Waals interactions between benzene and CrI_3 monolayer. During optimization, both the lattice constants and positions of all atoms are relaxed without any symmetry restriction until the Hellmann−Feynman force on each atom is less than 0.01 eV $Å^{-1}$. The convergent criterion for the total energy is set as 1×10^{-5} eV. To avoid interactions between two neighboring images, a vacuum space of 30 Å along the *z*-direction is adopted. To evaluate the thermodynamic stability of C_6H_6@CrI_3 structure, AIMD simulation was further employed. The AIMD simulation was performed under a constant temperature and volume (*NVT*) ensemble with a thermostat at 300 K by the Nosé−Hoover method,[43] and the simulation lasts for 3 ps with a time step of 1 fs.

3. RESULTS

3.1. Stability and Adsorption Geometry of Benzene on CrI_3. As shown in Figure 1a,b, the pristine CrI_3 monolayer has an I−Cr−I sandwich-like structure. The Cr atoms form a honeycomb 2D lattice. Each Cr atom is octahedrally surrounded by six I atoms, and each I atom connects two neighboring Cr atoms. To study the adsorption of an isolated benzene molecule on the surface of the CrI_3 monolayer, a 2 × 2 supercell, including 8 chromium atoms and 24 iodine atoms, was adopted, and total energy calculations were performed using a 3 × 3 × 1 *k*-point mesh. The distance between two adjacent benzene is around 10 Å and hence the interaction between them can be ignored. To determine the most stable configuration, as shown in Figure 1a, five possible adsorption sites (marked as I-top, Cr-top, H1, H2, and bridge sites) are taken into consideration which means that the center of benzene molecule is located at the top of I atom, Cr atom, the Cr−I bond, and the two hollow sites, respectively. Initial

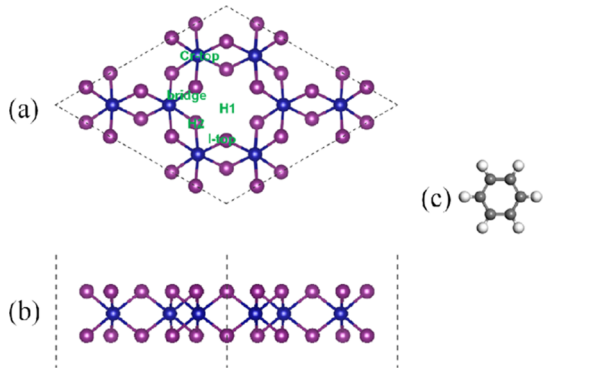

Figure 1. (a) Top view of CrI_3 monolayer. Inset labels represent different adsorption sites: I-top, Cr-top, bridge, and hollow sites H1, H2. (b) Side view of CrI_3 monolayer. (c) Structure of benzene molecule. The blue, purple, gray, and white balls represent Cr, I, C, and H atoms, respectively.

structures with the benzene perpendicular or parallel to the CrI_3 are all considered in our calculations. We find that the perpendicular ones have very similar adsorption energy of ∼0.2 eV, which is much higher than the parallel ones. In fact, after fully optimization, the benzene is not exactly parallel to the CrI_3 plane but is a bit tilted. The optimized structures for the nearly parallel configurations are shown in Figure 2.

The adsorption of benzene molecule on the surface does not break the framework of the CrI_3 monolayer. For all adsorption sites, the benzene molecule is found floating above the CrI_3 layer with a distance of around 3 Å, and there is no distinct chemical bonds between the benzene molecule and the CrI_3 monolayer. Adsorption of benzene does not result in any significant structural distortion of the monolayer. After full relaxation, total energy calculations were performed to get the adsorption energy which is defined as $E_{ads} = E_{total}(C_6H_6@CrI_3) - [E_{total}(CrI_3) + E_{total}(C_6H_6)]$, where $E_{total}(C_6H_6@CrI_3)$ is the total energy of CrI_3 with the adsorption of benzene, $E_{total}(CrI_3)$ is the total energy of a pristine CrI_3 monolayer, and $E_{total}(C_6H_6)$ is the total energy of an isolated benzene molecule. In this case, a negative value of adsorption energy indicates an exothermic reaction. A larger absolute value of adsorption energy indicates a more stable adsorption structure. The calculated adsorption energies for the five configurations are given in the first column in Table 1. The values of E_{ads} range from −0.35 to −0.42 eV. The I-top configuration has the largest absolute value of adsorption energy (−0.42 eV). Thus in the following, we focus on the I-top configuration of C_6H_6@CrI_3 systems.

We first investigate the effect of adsorption concentrations of benzene molecules. Here, the adsorption concentration is ranged from 0% (pristine CrI_3) to 100% (one benzene per primitive cell of CrI_3). The optimal I-top configuration was adopted in the calculations. The systems with different adsorption concentrations are denoted as $C_6H_6@(Cr_2I_6)_n$ (n = 4, 3, 2, and 1), where n represents the size of supercells of the CrI_3 monolayer. A smaller n represents a higher adsorption concentration. Structures with n = 4, 3, 2, and 1 are shown in Figures 2a, 3a,b, and 4a, respectively. Adsorption of benzene does not result in any significant structural distortion of the CrI_3 layer. For all considered adsorption patterns and adsorption concentrations, the change of the Cr−I bond length is smaller than 0.02 Å, and the Cr−I−Cr bonding angle is still very close to 90°. The calculated adsorption energy is

https://dx.doi.org/10.1021/acs.jpcc.0c06071
J. Phys. Chem. C 2020, 124, 22143−22149

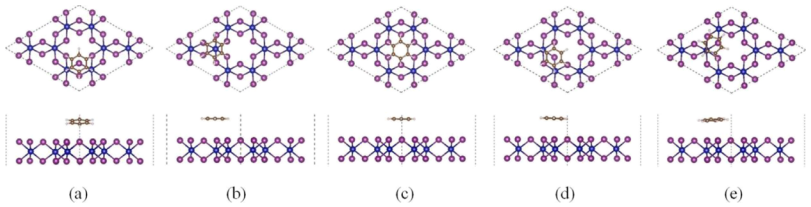

Figure 2. Top (upper panel) and side (bottom panel) view of optimized structures of benzene molecule adsorbed at different sites, that is (a) I-top, (b) Cr-top, (c) H1, (d) H2, and (e) bridge (one benzene molecule per 2 × 2 CrI_3 super cell). The blue, purple, gray and white balls represent Cr, I, C and H atoms, respectively.

Table 1. Adsorption Energy for Each Considered Adsorption configuration Shown in Figure 1 with Low (E_{ads1}) and High (E_{ads2}) Adsorption Concentrations

sites	E_{ads1} (eV)	E_{ads2} (eV)
I-top	−0.42	−0.50
Cr-top	−0.35	
H1	−0.39	−0.42
H2	−0.37	−0.47
Bridge	−0.40	−0.47

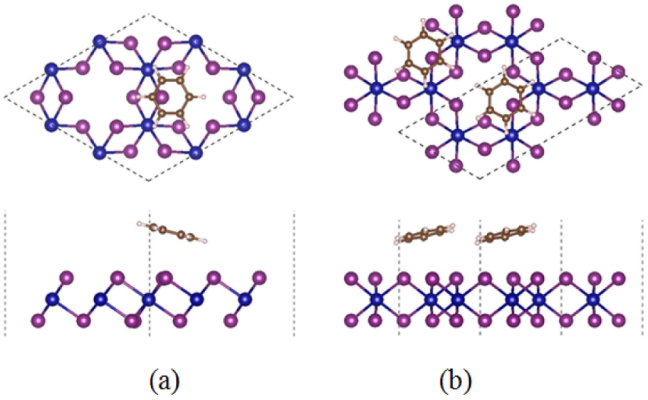

Figure 3. Top (upper panel) and side (bottom panel) view of optimized adsorption structure of benzene molecule at the I-top site with different adsorption concentrations: (a) $C_6H_6@(Cr_2I_6)_3$ and $C_6H_6@(Cr_2I_6)_2$.

−0.42, −0.42, −0.46, and −0.50 eV for n = 4, 3, 2, and 1, respectively. The cohesive energy of a single benzene in benzene crystal is 0.46 eV,[44] which is comparable to that of $C_6H_6@(Cr_2I_6)_2$ (0.46 eV) and is smaller than that of $C_6H_6@(Cr_2I_6)_1$ (0.50 eV). We can see that the absolute value of adsorption energy for these systems become even larger as the adsorption concentration increases. This phenomenon is quite interesting because generally the electrostatic repulsion among the adsorbed molecules become larger, and the adsorption energy should be smaller as the adsorption concentration increases. This implies that there is a strong interaction between benzene and the CrI_3 layer which becomes even stronger when the adsorption concentration increases. Thus, a great change on electronic and/or magnetic properties can be expected when the adsorption concentration is changed. To be rigorous, we have also calculated other four possible adsorption configurations for the $C_6H_6@Cr_2I_6$. After full relaxation, the Cr-top configuration always automatically converge into the bridge configuration. All structures and corresponding adsorption energies are shown in Figure 4 and second column of Table 1, respectively. The I-top site is again the most favored adsorption site. It is worth noting that the adsorption energy of benzene on silicene was theoretically reported to be 0.29 eV,[32] which is much smaller than that (0.50 eV) of benzene adsorbed on CrI_3. This indicates that CrI_3 might be a better candidate to detect or act as a sensor for gas benzene. In general, our results suggest that benzene can be strongly bounded to CrI_3, and hence, CrI_3 could be a better host material for benzene molecules, which makes it a potential candidate material for sensors as well as electronic device applications.

Before further discussions on the adsorption effects, it is necessary to check the stability of the calculated structure, which is crucial for its experimental fabrication and practical applications. The thermal stability of the I-top configuration is examined by AIMD simulations using a 2 × 2 supercell containing 44 atoms in total. During simulations, the benzene molecules slightly vibrate and rotate around their equilibrium position. After a simulation time of 3 ps, the adsorption configuration is still maintained. The variations of the total energy and temperature with time during simulations are plotted in Figure 5c in which there is no visible sudden change of the profiles. These suggest that the $C_6H_6@Cr_2I_6$ structure is thermally stable.

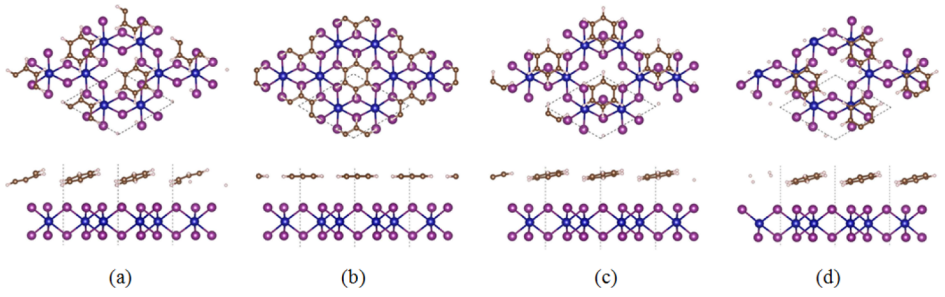

Figure 4. Top (upper panel) and side (bottom panel) view of optimized adsorption structures of $C_6H_6@Cr_2I_6$. (a) I-top, (b) H1, (c) H2, and (d) bridge adsorption configuration.

https://dx.doi.org/10.1021/acs.jpcc.0c06071
J. Phys. Chem. C 2020, 124, 22143−22149

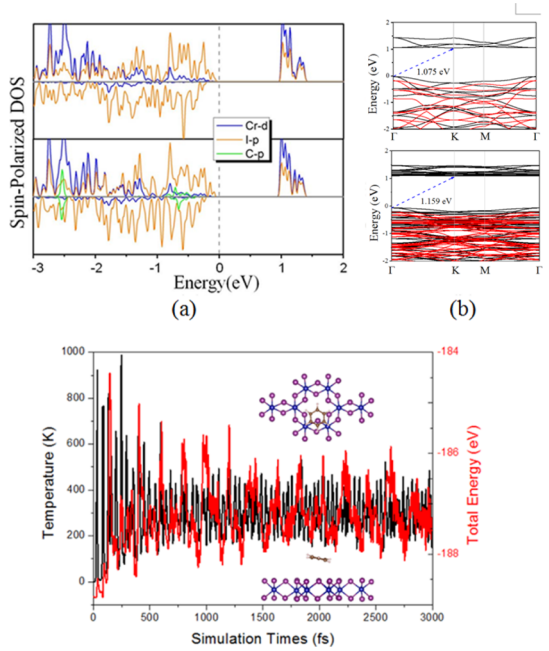

Figure 5. (a) PDOS of CrI_3 (upper) and $C_6H_6@Cr_2I_6$ (bottom). (b) Spin-polarized band structures of CrI_3 (upper) and $CrI_3@C_6H_6$ (bottom). The black (red) lines represent the spin-up (spin-down) bands. (c) AIMD evolutions of the total energy (red line) and temperature (black line) for the $C_6H_6@Cr_2I_6$ nanosheet. The inset structural snapshots are the full coverage structure after 3 ps at 300 K.

3.2. Effect of Adsorption of Benzene Molecules on Electronic and Magnetic Structures. Next, we investigate the effect of adsorption of benzene molecules on electronic and magnetic structures. In consistent with previous reports,[45] without considering the SOC effect, the band structure and partial density of states (PDOS), as shown in the upper panels of Figure 5a,b, indicate that the CrI_3 monolayer is a semiconductor with an indirect band gap of 1.08 eV. The valence bands and conduction bands near the Fermi level are mainly contributed by Cr-3d and I-5p orbitals. For $C_6H_6@Cr_2I_6$, the indirect band gap was maintained, and there is a visible contribution from C-p orbital of benzene around the Fermi level, as shown in the Figure 5a. This implies that the adsorption of benzene may greatly affect the electronic and magnetic properties of CrI_3. Adsorption concentration effects on the band structure of the monolayer CrI_3 is further investigated with including SOC effects. Figure 6 displays the electronic band structures of $C_6H_6@(Cr_2I_6)_n$ with different benzene concentrations (n = 3, 2, and 1). For n = 1, electronic band structures for other adsorption configurations are also given. We find that after including SOC, all structures are direct band gap semiconductors with the valence band maximum and conduction band minimum located at the Γ point. The band gaps of the I-top configurations for $C_6H_6@(Cr_2I_6)_3$, $C_6H_6@(Cr_2I_6)_2$, and $C_6H_6@Cr_2I_6$ are 0.71, 0.71, and 0.72 eV, respectively. The $C_6H_6@Cr_2I_6$ may exhibits an increase in luminescence quantum efficiency, which suggests its potential use for photostable markers and sensors in probing nanoscale dimensions.

The adsorption of benzene does not change the magnetic easy axis of CrI_3, that is, the magnetic easy axis is still along the out-of-plane direction after adsorbing benzene. The magnetic anisotropic energies (MAE = $E_{m//a} - E_{m//c}$) are calculated to be 0.77, 0.62, 0.57, 0.50, and 0.42 meV/Cr for $C_6H_6@(Cr_2I_6)_4$, $C_6H_6@(Cr_2I_6)_3$, $C_6H_6@(Cr_2I_6)_2$, and $C_6H_6@Cr_2I_6$, respectively. The MAE slightly decreases as the adsorption concentration of benzene increases.

3.3. Curie Temperature. In this section, we calculate the values of exchange energy (E_{ex}). The E_{ex} is the energy difference of stable antiferromagnetic (AFM) and FM states ($E_{ex} = E_{AFM} - E_{FM}$) per Cr ion. A positive value indicates a FM ground state. It is found that the FM states are lower in energy than the corresponding AFM states by 29, 30, 30, and 37 meV per Cr for $C_6H_6@(Cr_2I_6)_n$ with n = 4, 3, 2, and 1, respectively. The enhancement of E_{ex} induced by the adsorption of benzene can also be understood through a super-exchange mechanism.[48] First, the interaction between benzene and the CrI_3 layer is strong because of the large adsorption energy (up to 0.5 eV). Second, from the PDOS shown in Figure 5a, we find that there is a distinct contribution of C-p orbitals around the Fermi level, which also indicates an interaction between Cr-d and C-p orbitals. Third, the Cr−C−Cr bond angle is less than 90°, which also prefers an FM super-exchange interaction according to the Goodenough - Kanamori - Anderson (GKA) rules. Thus, the adsorption of benzene may provide extra FM super-exchange paths, which leads to an enhancement of FM coupling of CrI_3. T_C is a key parameter to the practical application of FM materials. Therefore, it is necessary to understand the behavior of the magnetism under finite temperature. Based on the Ising model which has been widely used, the T_C of $C_6H_6@Cr_2I_6$ can be estimated by using Monte Carlo (MC) simulations. The MC simulation is performed on the basis of the Metropolis method. A 30 × 30 hexagonal super lattice containing 1800 magnetic sites is used to mimic the 2D magnetic layer, and it is large enough to minimize the periodic constraints. Each spin randomly flips between up and down states during simulations. The average magnetization per unit cell and specific heat which is defined as $C_v = (\langle E^2\rangle - \langle E\rangle^2)/k_BT^2$ are taken after the system reaches its equilibrium state (with at least 10^5 iteration steps) at a given temperature.

The spin Hamiltonian can be written as

$$H = -\sum_{i,j} JS_iS_j$$

where the summation i runs over all Cr sites, j runs over the three nearest-neighbors of site i. J is the nearest-neighboring exchange parameter. The exchange-coupling parameter J can be extracted by mapping the total energies of FM and AFM states to the Ising model, namely, $J = E_{ex}/2zS^2$, where z = 3 is the coordination number for a honeycomb spin−lattice formed by Cr atoms in the CrI_3 sheet, S = 3/2 is the spin quantum number of each Cr atom, and $E_{ex} = E_{AFM} - E_{FM}$ is the exchange energy.[46] E_{ex} and J for the pristine unit CrI_3 are calculated to be 59 and 4 meV, respectively.[47] When benzene is adsorbed on the I-top site of the unit, E_{ex} and J increase to 74 and 5 meV, respectively.

As shown in Figure 7, the estimated T_C for $C_6H_6@Cr_2I_6$ is 65 K, which is larger by ∼44% than the pristine CrI_3 monolayer (∼45 K) and is very close to the liquid nitrogen temperature (77 K). On the basis of the mean field theory, the T_C can also be estimated by the equation: $T_C^{MFT} = 2J/3k_B$. Using this method, the T_C for pristine CrI_3 and $C_6H_6@Cr_2I_6$ is estimated to be 69.6 and 87.0 K, respectively. These values are larger than those from MC simulations (45 and 65 K). It is worth noting that the mean field theory may usually

https://dx.doi.org/10.1021/acs.jpcc.0c06071
J. Phys. Chem. C 2020, 124, 22143−22149

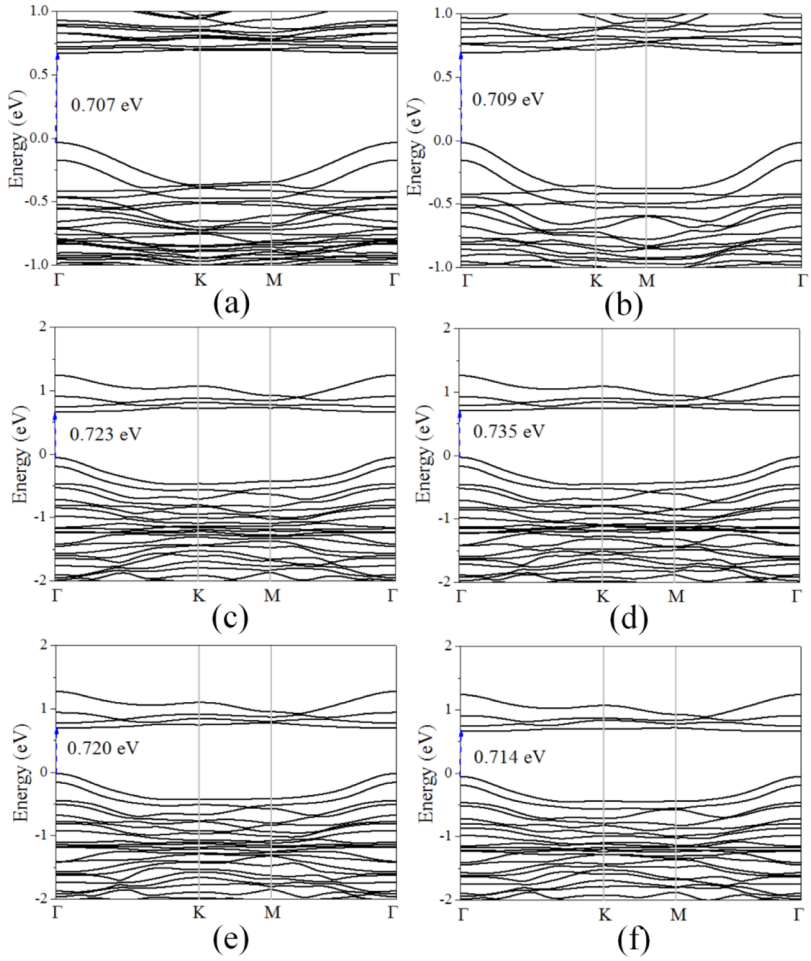

Figure 6. PBE + SOC electronic band structures of $C_6H_6@(Cr_2I_6)_n$ with different benzene concentrations: (a) n = 3 and (b) n = 2 and the high concentration (n = 1) at different adsorption sites (c) I-top, (d) H1, (e) H2, and (f) bridge site.

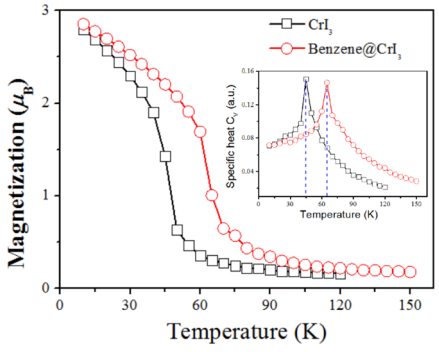

Figure 7. Magnetization with respect to temperature for the CrI_3 and $C_6H_6@Cr_2I_6$, and the inset shows the corresponding specific heat C_v.

overestimate the T_C.[49] Nevertheless, the adsorption of benzene can indeed enhance the FM couplings of CrI_3.

3.4. Effect of Adsorption of Benzene Molecule on Optical Absorption. In experiments, an important performance indicator of 2D semiconductor materials is the optical absorption. To investigate this possibility, we calculated the frequency-dependent dielectric function from the summation over pairs of occupied and empty states without considering the local field effects,[49] and then, the absorption coefficients as a function of photon energy were evaluated. The optical absorption coefficients within the xy plane and along the z-direction of the pristine and C_6H_6 adsorbed CrI_3 compounds are shown in Figure 8a,b, respectively. Due to the different dielectric responses in different directions caused by the geometric configuration state, an obvious anisotropic feature is observed. The optical absorption coefficient along the x/y direction is larger than the corresponding results within the z-direction for almost all materials except for pristine CrI_3. In the x/y direction, compared with CrI_3, there is an enhanced absorption peak at about 5−5.2 eV with an absorption intensity as high as 5×10^5 cm^{-1} for $C_6H_6@Cr_2I_6$. In the z-direction, the optical absorption of CrI_3 shows a strong absorption peak at about 1.7 eV and other peaks at around 3 and 5 eV. The other materials have strong absorption peaks at about 3−3.2 and 4.4−4.7 eV. It is worth mentioning that the obvious anisotropic feature implies that these monolayers can be candidate materials for designing an optical waveguide polarizer. A polarizer is one of the most important devices in optics, which only transmits light in one polarization direction by absorbing or reflecting light in the other polarization direction.[50]

4. CONCLUSIONS

In summary, by means of first-principles calculations, we theoretically studied the adsorption mechanism and electronic and magnetic properties of benzene molecules adsorbed on the surface of the 2D FM semiconductor CrI_3. The adsorption

https://dx.doi.org/10.1021/acs.jpcc.0c06071
J. Phys. Chem. C 2020, 124, 22143−22149

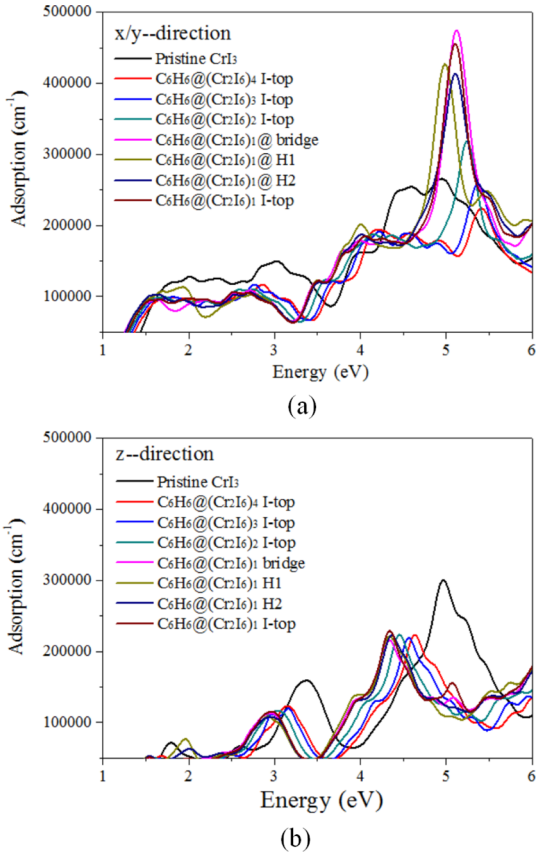

Figure 8. Optical absorption coefficient along (a) *xy* plane and (b) *z*-direction of the pristine CrI_3 and $C_6H_6@(Cr_2I_6)_n$ compounds in energy.

energy ranges from −0.42 to −0.50 eV as the adsorption concentration of benzene molecules ranges from $C_6H_6@(Cr_2I_6)_4$ to $C_6H_6@Cr_2I_6$. It is found that the adsorption of benzene molecules can enhance the optical absorption and FM couplings of the CrI_3 monolayer. As our results suggest, future engineering of the electronic and magnetic properties of CrI_3 may include manipulating the surface decoration by organic molecules. Such a method can also be used to study other 2D layered materials. The high anisotropy in optical absorption indicates a high polarization sensitivity and provides a good opportunity for designing an optical waveguide polarizer. We are looking forward to future experimental evidences.

AUTHOR INFORMATION

Corresponding Authors

Chengxi Huang − *Department of Applied Physics and Institution of Energy and Microstructure, Nanjing University of Science and Technology, Nanjing, Jiangsu 210094, P. R. China;* orcid.org/0000-0003-1491-3954; Email: dawnhcx@gmail.com

Erjun Kan − *Department of Applied Physics and Institution of Energy and Microstructure, Nanjing University of Science and Technology, Nanjing, Jiangsu 210094, P. R. China;* orcid.org/0000-0003-0433-4190; Email: ekan@njust.edu.cn

Authors

Min Lu − *Department of Applied Physics and Institution of Energy and Microstructure, Nanjing University of Science and Technology, Nanjing, Jiangsu 210094, P. R. China*

Qiushi Yao − *Department of Physics and Shenzhen Institute for Quantum Science and Technology, Southern University of Science and Technology, Shenzhen 518055, China*

Qiongyu Li − *Department of Applied Physics and Institution of Energy and Microstructure, Nanjing University of Science and Technology, Nanjing, Jiangsu 210094, P. R. China*

Chuanyun Xiao − *Department of Applied Physics and Institution of Energy and Microstructure, Nanjing University of Science and Technology, Nanjing, Jiangsu 210094, P. R. China*

Complete contact information is available at: https://pubs.acs.org/10.1021/acs.jpcc.0c06071

Author Contributions

The manuscript was written through contributions of all authors. All authors have given approval to the final version of the manuscript.

Notes

The authors declare no competing financial interest.

ACKNOWLEDGMENTS

The work is supported by the NSFC (51522206 and 11774173) and the Fundamental Research Funds for the Central Universities (no. 30915011203). C.H. and E.K. acknowledge the support from the Tianjing Supercomputer Centre and Shanghai Supercomputer Center.

REFERENCES

(1) Geim, A. K.; Novoselov, K. S. The Rise of Graphene. *Nat. Mater.* **2007**, *6*, 183−191.

(2) Geim, A. K. Graphene: Status and Prospects. *Science* **2009**, *324*, 1530−1534.

(3) Novoselov, K. S.; Geim, A. K.; Morozov, S. V.; Jiang, D.; Zhang, Y.; Dubonos, S. V.; Grigorieva, I. V.; Firsov, A. A. Electric Field Effect in Atomically Thin Carbon Films. *Science* **2004**, *306*, 666−669.

(4) Han, W.-Q.; Wu, L.; Zhu, Y.; Watanabe, K.; Taniguchi, T. Structure of Chemically Derived Mono- and Few-Atomic-Layer Boron Nitride Sheets. *Appl. Phys. Lett.* **2008**, *93*, 223103−223105.

(5) Wang, Q. H.; Kalantar-Zadeh, K.; Kis, A.; Coleman, J. N.; Strano, M. S. Electronics and Optoelectronics of Two-Dimensional Transition Metal Dichalcogenides. *Nat. Nanotechnol.* **2012**, *7*, 699−712.

(6) Youngblood, N.; Chen, C.; Koester, S. J.; Li, M. Waveguide-Integrated Black Phosphorus Photodetector with High Responsivity and Low Dark Current. *Nat. Photon.* **2015**, *9*, 247−252.

(7) Fert, A. Nobel Lecture: Origin, Development, and Future of Spintronics. *Rev. Mod. Phys.* **2008**, *80*, 1517−1530.

(8) Mermin, N. D.; Wagner, H. Absence of Ferromagnetism or Antiferromagnetism in One- or Two-dimensional Isotropic Heisenberg Models. *Phys. Rev. Lett.* **1966**, *17*, 1133−1136.

(9) Liu, J.; Sun, Q.; Kawazoe, Y.; Jena, P. Exfoliating Biocompatible Ferromagnetic Cr-trihalide Monolayers. *Phys. Chem. Chem. Phys.* **2016**, *18*, 8777−8784.

(10) Du, A.; Sanvito, S.; Smith, S. C. First-principles Prediction of Metal-free Magnetism and Intrinsic Half-metallicity in Graphitic Carbon Nitride. *Phys. Rev. Lett.* **2012**, *108*, 197207.

(11) Wang, B.; Wu, Q.; Zhang, Y.; Guo, Y.; Zhang, X.; Zhou, Q.; Dong, S.; Wang, J. High Curie-Temperature Intrinsic Ferromagnetism and Hole Doping-Induced Half-Metallicity in Two-Dimensional Scandium Chlorine Monolayer. *Nanoscale Horiz.* **2018**, *3*, 551−555.

(12) Sun, Y.; Zhuo, Z.; Wu, X.; Yang, J. Room-temperature Ferromagnetism in Two-dimensional Fe_2Si Nanosheet with Enhanced Spin-polarization Ratio. *Nano Lett.* **2017**, *17*, 2771−2777.
(13) Chen, Q.; Ouyang, Y.; Yuan, S.; Li, R.; Wang, J. Uniformly Wetting Deposition of Co atoms on MoS_2 Monolayer: A Promising Two-dimensional Robust Half-metallic Ferromagnet. *ACS Appl. Mater. Interfaces* **2014**, *6*, 16835−16840.
(14) Gong, C.; Li, L.; Li, Z.; Ji, H.; Stern, A.; Xia, Y.; Cao, T.; Bao, W.; Wang, C.; Wang, Y.; et al. Discovery of Intrinsic Ferromagnetism in Two-Dimensional van der Waals Crystals. *Nature* **2017**, *546*, 265−269.
(15) Huang, B.; Clark, G.; Navarro-Moratalla, E.; Klein, D. R.; Cheng, R.; Seyler, K. L.; et al. Layer-Dependent Ferromagnetism in a van der Waals Crystal Down to The Monolayer Limit. *Nature* **2017**, *546*, 270−273.
(16) Jiang, S.; Li, L.; Wang, Z.; Mak, K. F.; Shan, J. Controlling magnetism in 2D CrI_3 by Electrostatic Doping. *Nat. Nanotechnol.* **2018**, *13*, 549−553.
(17) Webster, L.; Yan, J. A. Strain-tunable Magnetic Anisotropy in Monolayer $CrCl_3$, $CrBr_3$, and CrI_3. *Phys. Rev. B: Condens. Matter Mater. Phys.* **2018**, *98*, 144411.
(18) Li, T.; Jiang, S.; Sivadas, N.; Wang, Z.; Xu, Y.; Weber, D.; Goldberger, J. E.; Watanabe, K.; Taniguchi, T.; Fennie, C. J.; et al. Pressure-controlled Interlayer Magnetism in Atomically Thin CrI_3. *Nat. Mater.* **2019**, *18*, 1303−1308.
(19) Kang, S.; Kang, S.; Yu, J. Effect of Coulomb Interactions on the Electronic and Magnetic Properties of Two-Dimensional $CrSiTe_3$ and $CrGeTe_3$ Materials. *J. Electron. Mater.* **2019**, *48*, 1441−1445.
(20) Shang, J.; Tang, X.; Tan, X.; Du, A.; Liao, T.; Smith, S. C.; Gu, Y.; Li, C.; Kou, L. Stacking-Dependent Interlayer Magnetic Coupling 2D CrI_3/$CrGeTe_3$ Nanostructures for Spintronics. *ACS Appl. Nano Mater.* **2020**, *3*, 1282−1288.
(21) Liu, W.; Xu, Y. Magnetic two-dimensional systems. *Curr. Opin. Solid State Mater. Sci.* **2016**, *20*, 388−395.
(22) Kim, J.; Yun, W. S.; Lee, J. D. Optical Absorption of Armchair MoS2 Nanoribbons: Enhanced Correlation Effects in the Reduced Dimension. *J. Phys. Chem. C* **2015**, *119*, 13901−13906.
(23) Wang, Q. H.; Kalantar-Zadeh, K.; Kis, A.; Coleman, J. N.; Strano, M. S. Electronics and Optoelectronics of Two-dimensional Transition Metal Dichalcogenides. *Nat. Nanotechnol.* **2012**, *7*, 699−712.
(24) Lopez-Sanchez, O.; Lembke, D.; Kayci, M.; Radenovic, A.; Kis, A. Ultrasensitive Photodetectors Based on Monolayer MoS_2. *Nat. Nanotechnol.* **2013**, *8*, 497−501.
(25) Zhang, W.-B.; Qu, Q.; Zhu, P.; Lam, C.-H. Robust Intrinsic Ferromagnetism and Half Semiconductivity in Stable Two-Dimensional Single-Layer Chromium Trihalides. *J. Mater. Chem. C* **2015**, *3*, 12457−12468.
(26) Samuels, A. J.; Carey, J. D. Molecular Doping and Bandgap Opening of Bilayer Graphene. *ACS Nano* **2013**, *7*, 2790−2799.
(27) Tang, Q.; Zhou, Z.; Chen, Z. Molecular Charge Transfer: A Simple and Effective Route to Engineer the Band Structures of BN Nanosheets and Nanoribbons. *J. Phys. Chem. C* **2011**, *115*, 18531−18537.
(28) Jing, Y.; Tan, X.; Zhou, Z.; Shen, P. Tuning Electronic and Optical Properties of MoS_2 Monolayer via Molecular Charge Transfer. *J. Mater. Chem. A* **2014**, *2*, 16892−16897.
(29) Dey, S.; Matte, H. S. S. R.; Shirodkar, S. N.; Waghmare, U. V.; Rao, C. N. R. Charge-transfer Interaction Between Few-layer MoS_2 and Tetrathiafulvalene. *Chem.—Asian J.* **2013**, *8*, 1780−1784.
(30) Kiriya, D.; Tosun, M.; Zhao, P.; Kang, J. S.; Javey, A. Airstable Surface Charge Transfer Doping of MoS_2 by Benzyl Viologen. *J. Am. Chem. Soc.* **2014**, *136*, 7853−7856.
(31) Kaloni, T. P.; Schreckenbach, G.; Freund, M. S. Large Enhancement and Tunable Band Gap in Silicene by Small Organic Molecule Adsorption. *J. Phys. Chem. C* **2014**, *118*, 23361−23367.
(32) Wang, Y.-p.; Ji, W.-x.; Zhang, C.-w.; Li, S.-s.; Li, F.; Li, P.; Ren, M.-j.; Chen, X.-l.; Yuan, M.; Wang, P.-j. Enhanced Band Gap Opening in Germanene by Organic Molecule Adsorption. *Mater. Chem. Phys.* **2016**, *173*, 379−384.
(33) Xia, F.; Xiong, S.; He, Y.; Shao, Z.; Zhang, X.; Jie, J. Tuning the Electronic and Optical Properties of Monolayer As, Sb and Bi via Surface Charge Transfer Doping. *J. Phys. Chem. C* **2017**, *121*, 19530−19537.
(34) Kresse, G.; Furthmüller, J. Efficient Iterative Schemes for ab initio Total-Energy Calculations Using a Plane-Wave Basis Set. *Phys. Rev. B: Condens. Matter Mater. Phys.* **1996**, *54*, 11169−11186.
(35) Perdew, J. P.; Burke, K.; Ernzerhof, M. Generalized Gradient Approximation Made Simple. *Phys. Rev. Lett.* **1996**, *77*, 3865−3868.
(36) Kresse, G.; Joubert, D. From Ultrasoft Pseudopotentials to the Projector Augmented-Wave Method. *Phys. Rev. B: Condens. Matter Mater. Phys.* **1999**, *59*, 1758−1775.
(37) Dudarev, S. L.; Botton, G. A.; Savrasov, S. Y.; Humphreys, C. J.; Sutton, A. P. Electron-Energy-Loss Spectra and the Structural Stability of Nickel Oxide: An LSDA+U Study. *Phys. Rev. B: Condens. Matter Mater. Phys.* **1998**, *57*, 1505−1509.
(38) Monkhorst, H. J.; Pack, J. D. Special Points for Brillonin-Zone Integrations. *Phys. Rev. B: Condens. Matter Mater. Phys.* **1976**, *13*, 5188−5192.
(39) Chadi, D. J.; Cohen, M. L. Special Points in the Brillouin Zone. *Phys. Rev. B: Condens. Matter Mater. Phys.* **1973**, *8*, 5747−5753.
(40) Baldereschi, A.; Tosatti, E. Mean-Value Point and Dielectric Proyerties of Semiconductors and Insulators. *Phys. Rev. B: Condens. Matter Mater. Phys.* **1978**, *17*, 4710−4717.
(41) Grimme, S. Semiempirical GGA-type Density Functional Constructed with a Long-Range Dispersion Correction. *J. Comput. Chem.* **2006**, *27*, 1787−1799.
(42) Li, Y.; Chen, Z. XH/π (X = C, Si) Interactions in Graphene and Silicene: Weak in Strength, Strong in Tuning Band Structures. *J. Phys. Chem. Lett.* **2013**, *4*, 269−275.
(43) Bucher, D.; Pierce, L. C. T.; Mccammon, J. A.; Markwick, P. R. L. On the Use of Accelerated Molecular Dynamics to Enhance Configurational Sampling in Ab Initio Simulations. *J. Chem. Theory Comput.* **2011**, *7*, 890−897.
(44) Bludsky, O.; Rubes, M.; Soldan, P. Ab initio investigation of intermolecular interactions in solid benzene. *Phys. Rev. B: Condens. Matter Mater. Phys.* **2008**, *77*, 092103.
(45) Wu, Z.; Yu, J.; Yuan, S. Strain-tunable Magnetic and Electronic Properties of Monolayer CrI_3. *Phys. Chem. Chem. Phys.* **2019**, *21*, 7750−7755.
(46) Zhuang, H. L.; Xie, Y.; Kent, P. R. C.; Ganesh, P. Computational Discovery of Ferromagnetic Semiconducting Single-layer. *Phys. Rev. B: Condens. Matter Mater. Phys.* **2015**, *92*, 035407.
(47) Huang, C.; Feng, J.; Wu, F.; Ahmed, D.; Huang, B.; Xiang, H.; Deng, K.; Kan, E. Toward Intrinsic Room-Temperature Ferromagnetism in Two-Dimensional Semiconductors. *J. Am. Chem. Soc.* **2018**, *140*, 11519−11525.
(48) He, J.; Ding, G.; Zhong, C.; Li, S.; Li, D.; Zhang, G. Remarkably Enhanced Ferromagnetism in Super-exchange Governed $Cr_2Ge_2Te_6$ Monolayer via Molecular Adsorption. *J. Mater. Chem. C* **2019**, *7*, 5084−5093.
(49) Xiang, H. J.; Huang, B.; Li, Z. Y.; Wei, S. H.; Yang, J. L.; Gong, X. G. Ordered Semiconducting Nitrogen-graphene Alloys. *Phys. Rev. X* **2012**, *2*, 011003.
(50) Sinha, R. K.; Kalra, Y. Design of Optical Waveguide Polarizer Using Photonic Band Gap. *Opt. Express* **2006**, *14*, 10790−10794.

https://dx.doi.org/10.1021/acs.jpcc.0c06071
J. Phys. Chem. C 2020, 124, 22143−22149